Colliding solitary waves in quark gluon plasmas

Azam Rafiei and Kurosh Javidan*
Department of Physics, Faculty of Science, Ferdowsi University of Mashhad, 91775-1436 Mashhad, Iran
(Received 28 April 2016; revised manuscript received 12 August 2016; published 20 September 2016)

We study the head-on collision of propagating waves due to perturbations in quark gluon plasmas. We use the Massachusetts Institute of Technology bag model, hydrodynamics equation, and suitable equation of state for describing the time evolution of such localized waves. A nonlinear differential equation is derived for the propagation of small amplitude localized waves using the reductive perturbation method. We show that these waves are unstable and amplitude of the left-moving (right-moving) wave increases (decreases) after the collision, and so they reach the borders of a quark gluon plasma fireball with different amplitudes. Indeed we show that such arrangements are created because of the geometrical symmetries of the medium.

DOI: 10.1103/PhysRevC.94.034904

I. INTRODUCTION

There are acceptable theoretical reasons and experimental evidence indicating the existence of a new state of matter with high temperature and/or high density, called quark gluon plasmas (QGPs). According to the standard model of particle physics, it is expected that, a few microseconds after the Big Bang, the universe was made from deconfined quarks in the state of the QGPs [1–4]. Another astronomical situation in which one expects to find signatures of the QGPs is at the core of compact stars [5,6]. For reconstruction of this state of matter in terrestrial laboratories, the Relativistic Heavy Ion Collider (RHIC) and the Large Hadron Collider (LHC) have been utilized. In these machines, when two nuclei with relativistic velocities collide, most of their nucleons interact with each other instantly, and many partons are produced. Depending on the primary energy per nucleon, two different kinds of deconfined QGP phases with chiral symmetry can be created. It is possible that a QGP phase produces with large baryon number density at low incident energy per nucleon [7]. The other possibility is creating a QGP phase with high temperature and a very small net baryon number at very high energy per nucleon [7–9]. Afterwards the system expands and experiences a phase transition to hadronic gas while the density decreases more and more due to this expansion. The collision rate decreases in time, and the system finally reaches a situation in which the collision rate is not large enough to preserve the chemical equilibrium. But there are still hadronic interactions, until finally the produced particles continue their way without further interactions [2].

Nowadays investigation of the QGP behavior is one of the main objectives of RHIC and LHC. In order to study the evolution of the universe before the first few microseconds, we have to extrapolate cosmological models. In this way quark gluon plasmas play the role of initial conditions for the next step of understanding the evolution of the universe. It may be noted that any fluctuation at QGPs can affect the results.

Since a QGP has very low viscosity [10], it behaves like a perfect fluid [11,12]. Relativistic hydrodynamical equations are used for the space-time evolution of the matter, produced in the high-energy nuclear collisions [13–15]. Also by using the hydrodynamics equations we can investigate the evolution of the observable perturbations at head-on collisions too [16,17]. There are four different sources of density fluctuations which create localized waves propagating in the medium. Quantum fluctuations in the densities of two colliding nuclei supplemented with energy fluctuations are called initial-state fluctuations [18,19]. Local thermal fluctuations of the energy density and flow velocity produce hydrodynamic fluctuations [20]. Energy loss due to propagation of energetic partons causes hard process fluctuations. Finally there are event-by-event fluctuations during and after the freeze-out stage which are called freeze-out fluctuations [21,22]. So these fluctuations accompanied by macroscopic fluctuations in the other stage of the collision can affect global observations [3,23]. In a microscopic point of view the evolution of the fluctuations is evaluated using the perturbations through the Boltzmann equation by Sarwar and Alam [3]. It is worth noting that the fluctuations have been presented like boundaries of the critical end point in the quantum chrome-dynamics (QCD) phase transition [24,25]. Such perturbations are able to create nonlinear localized waves in the medium which can be detected and studied during the evolution of the system. Therefore, the propagation of nonlinear waves and their collisions is a very attractive subject.

Using the conservation of energy-momentum equations and the conservation of baryon density on the evolution of localized perturbations led us to a nonlinear equation which we called the "breaking wave equation" in some literature [21]. The breaking wave equation is similar to the Korteweg–de Vries (KdV) equation without its third derivative term, which makes the dispersion effect. Because of neglecting the charge of quarks in hydrodynamic description of a QGP that omits the Laplace equation, there is no dispersion expression in the equation. However the nonlinear term, which is originated from nonlinear terms of the conservation of baryon density and the Euler equations, exists in derived wave equation. As seen in nuclear matter the KdV equation establishes a solitary wave solution in the medium [26–28]. In these situations perturbations on the nuclear density are able to propagate like a nondamped wave [29]. Unfortunately the breaking wave equation has no known exact solution. Therefore to solve this equation one can use numerical simulations with the KdV soliton localized solution as the initial conditions [30].

*javidan@um.ac.ir

 ©2016 American Physical Society

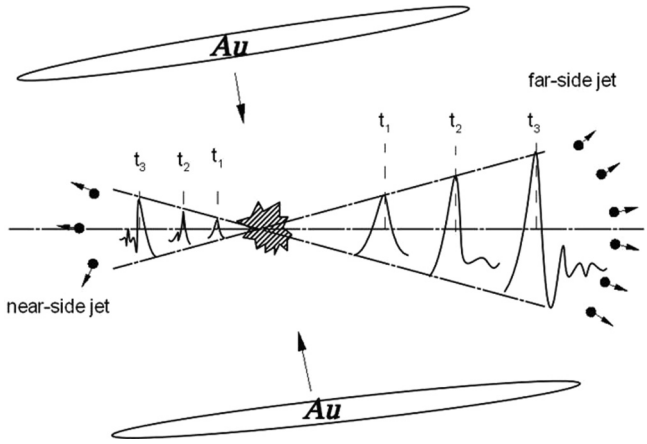

FIG. 1. Dijet production in hot and cold quark gluon plasmas.

There are few theories for describing the QGP matter. The lattice gauge theory is used at low densities and high temperatures without the ability to explore the color-superconducting phase structure. The weak-coupling theory using a schematic shows the color-flavor- locked phase takes place at higher densities, however this method cannot be utilized at high temperatures. According to the Nambu-Jona-Lasinio model one gluon at strong interaction is replaced by a four-fermion interaction.

Besides the energy momentum of the particles, there is another excess energy of confinement which can be described by a suitable mean-field theory. The Massachusetts Institute of Technology (MIT) bag model is a simple and suitable theory for explaining this energy. It is shown that confinement energy plays an important role in the evolution of small amplitude localized waves [21]. In this paper we use the well-known MIT bag model for completing the equation of state (EoS).

There are many experimental observations of colliding localized waves in the evolution of a fireball produced after the heavy ion collisions. Figure 1 presents a schematic for the creation of such waves.

Head-on collisions of solitary waves in a degenerate hadron gas have been investigated before. To the best knowledge of the authors, there are no archival publications considering the detailed behavior of such dijets. In this paper we try to explain another source for creating such back-to-back jets during the evolution of the produced QGP after the heavy ion collisions. Recently, we have studied the nonrelativistic dynamics of high-density hadronic gas with shear and bulk viscosities in the cold hadronic matter [31]. Propagation and head-on collisions of localized waves in such media have been investigated using the hadronic gas equation of state which mostly was applied in cold QGPs as exists in superdense astronomical objects. We showed that these waves can travel longer distances before changing into deformed profiles and totally dissolving in the viscous media in comparison with inviscid environments. Anyway the traveling distances of such waves are small. In the present paper we discuss the relativistic dynamics of localized multisolutions in high- (and low-) temperature quark gluon plasmas. The results help us to explain the creation of dijets in heavy ion collisions.

In the next section we will introduce the hydrodynamic equations for the system. As previously mentioned, these equations explain the perfect fluid behavior created in heavy ion collisions. The bag model is presented in Sec. III. Then the equations which describe the details of head-on collisions in QGPs are obtained in Sec. IV. The numerical calculation for the evolution of two QGP colliding waves is investigated in Secs. V and VI. Finally conclusions are discussed in Sec. VII.

II. RELATIVISTIC HYDRODYNAMICS

Observations in relativistic heavy ion collisions have confirmed the existence of a new state of matter that behaves similar to a perfect fluid. For describing the evolution of this state of matter one can use the relativistic hydrodynamics. Information of the system is encoded in the thermodynamic properties and its EoS [32,33].

Produced QGPs in heavy ion collisions are extremely high-temperature media, consisting of high-energy ingredients. The energy-momentum tensor of the system by considering natural units $c = 1$, $\hbar = 1$, and $k_B = 1$ (k_B is Boltzmann's constant) becomes

$$T_{\mu\nu} = (\varepsilon + p)u_\mu u_\nu - p g_{\mu\nu}, \tag{1}$$

where u^ν is the four-vector velocity with $u^0 = \gamma$ and $\vec{u} = \gamma\vec{v}$. γ is the Lorentz factor given by $\gamma = (1 - v^2)^{-1/2}$. $\vec{v} = \vec{v}(t,r,\varphi,z)$ is the velocity of matter in a cylindrical coordinate, and therefore $u^\nu u_\nu = 1$. The energy density and pressure of the system are ε and p, respectively. The energy-momentum conservation equation is as follows:

$$\partial_\nu T^\nu_\mu = 0. \tag{2}$$

The relativistic Euler equation is obtained from components of Eq. (2) perpendicular to the direction of u^ν as

$$\frac{\partial\vec{v}}{\partial t} + (\vec{v}\cdot\vec{\nabla})\vec{v} = -\frac{1}{(\varepsilon + p)\gamma^2}(\vec{\nabla}p + \vec{v}). \tag{3}$$

Conservation of the baryon density is achieved from the relative continuity equation,

$$\partial_\nu j^\nu_B = 0. \tag{4}$$

Since $j^\nu_B = u^\nu\rho_B$, so modification of the continuity equation leads to

$$\frac{\partial\rho_B}{\partial t} + \gamma^2 v\rho_B\left(\frac{\partial v}{\partial t} + \vec{v}\cdot\vec{\nabla}v\right) + \vec{\nabla}\cdot(\rho_B\vec{v}) = 0. \tag{5}$$

Multiplying the conservation Eq. (2) with u^ν the following equation is earned [32]:

$$(\varepsilon + p)\partial_\mu u^\mu + u^\mu\partial_\mu\varepsilon = 0. \tag{6}$$

Now we need to use the thermodynamic equation of the system. We use the Gibbs relation,

$$\varepsilon + p = Ts + \mu_B\rho_B, \tag{7}$$

and the first law of thermodynamics,

$$d\varepsilon = Tds + \mu_B d\rho_B. \tag{8}$$

Recall that the produced QGP in RHIC involves high temperatures and nearly zero net baryon density, so the

chemical potential is equivalent to zero [32]. Therefore the last term in Eqs. (7) and (8) is neglected. Placing (7) and (8) into Eq. (6) we obtain

$$Ts(\partial_\mu u^\mu) + Tu^\mu(\partial_\mu s) = 0. \tag{9}$$

By eliminating the temperature in (9), the conservation of the entropy density resulted as we expected for the perfect fluid as

$$\partial_\nu(su^\nu) = 0. \tag{10}$$

Similar to Eq. (4) we can write the following equation from (10):

$$\frac{\partial s}{\partial t} + \gamma^2 vs\left(\frac{\partial v}{\partial t} + \vec{v}\cdot\vec{\nabla}v\right) + \vec{\nabla}\cdot(s\vec{v}) = 0. \tag{11}$$

At this stage we do not have a complete set of equations to calculate the evolution of the QGP system. Indeed we need another equation which should be taken as the equation of state of the system, which will be discussed in the next section.

III. BAG MODEL DESCRIPTION OF THE QGP

The equation of state for the QGP system can be derived using the MIT bag model. This model successfully describes the QGP as an ideal gas of noninteracting quarks and gluons. Inside the bag, quarks are treated as a noninteracting gas of quarks moving freely, and interactions with gluons are not taken into account. The bag constant $B_{\rm bag}$ represents the effects of confinement in this model as the needed energy to create a bag in the QCD vacuum [21]. The confinement boundary condition in the MIT bag model corresponds to the zero value for the quark mass inside the bag but infinity at the boundary and outside the bag [8,30,34].

Due to the MIT bag model the equation of state for the QGP as a perfect fluid accompanied by the bag constant $B_{\rm bag}$ is obtained as a function of baryon density, i.e., $p = p(\rho_B)$ and $\varepsilon = \varepsilon(\rho_B)$. For this purpose the baryon density arising from quarks and antiquarks is introduced as

$$\rho_B = \frac{1}{3}\frac{\gamma_Q}{(2\pi)^3}\int d^3k[n_{\vec{k}} - \bar{n}_{\vec{k}}], \tag{12}$$

where

$$n_{\vec{k}} \equiv n_{\vec{k}}(T) = \frac{1}{1 + e^{[k-(1/3)\mu]/T}}, \tag{13}$$

and

$$\bar{n}_{\vec{k}} \equiv \bar{n}_{\vec{k}}(T) = \frac{1}{1 + e^{[k+(1/3)\mu]/T}}. \tag{14}$$

Henceforth μ represents the baryon chemical potential. At zero temperature as the compact stars, the baryon density is equal to

$$\rho_B = \frac{2}{3\pi^2}k_F^3, \tag{15}$$

where k_F displays the highest occupied level. Now the recognized relations for the energy density and pressure are obtained from the following expressions:

$$\varepsilon = B_{\rm bag} + \frac{\gamma_G}{(2\pi)^3}\int d^3kk(e^{k/T} - 1)^{-1} + \frac{\gamma_Q}{(2\pi)^3}\int d^3kk[n_{\vec{k}} + \bar{n}_{\vec{k}}], \tag{16}$$

and

$$p = -B_{\rm bag} + \frac{1}{3}\left\{\frac{\gamma_G}{(2\pi)^3}\int d^3kk(e^{k/T} - 1)^{-1} + \frac{\gamma_Q}{(2\pi)^3}\int d^3kk[n_{\vec{k}} + \bar{n}_{\vec{k}}]\right\}, \tag{17}$$

where the statistical factor for the gluons is obtained by considering eight colors and the two-polarization $\gamma_G = 16$ and for quarks involving two flavors, two spins, and three colors $\gamma_Q = 12$.

For a combination of the above two expressions we get the qualified relations,

$$3(p + B_{\rm bag}) = \varepsilon - B_{\rm bag} = \frac{8\pi^2}{15}T^4 + \frac{6}{\pi^2}\int_0^\infty dkk^3[n_{\vec{k}} + \bar{n}_{\vec{k}}], \tag{18}$$

and

$$p = \tfrac{1}{3}\varepsilon - \tfrac{4}{3}B_{\rm bag}, \tag{19}$$

and the speed of sound is obtained as

$$c_s^2 = \frac{\partial p}{\partial \varepsilon} = \frac{1}{3}. \tag{20}$$

As previously mentioned, considering $\rho_B = 0$ for the high-temperature region created at the center of the heavy ion collision area, Eqs. (13) and (14) are identical, i.e. $(n_{\vec{k}} = \bar{n}_{\vec{k}} = \frac{1}{1+e^{k/T}})$ and replacing them in Eq. (18) we arrive at

$$3(p + B_{\rm bag}) = \varepsilon - B_{\rm bag} = \frac{37}{30}\pi^2T^4. \tag{21}$$

Now from thermodynamic relation for entropy density $s = (\partial p/\partial T)_V$, we have

$$s = \frac{\partial}{\partial T}\left(-B_{\rm bag} + \frac{37}{90}\pi^2T^4\right) = 4\frac{37}{90}\pi^2T^3. \tag{22}$$

For dense stars the selection for the bag constant is equal to $B_{\rm bag}^{1/4} = 170\,{\rm MeV}$ [35]. For convenience, $T_{\rm bag}$ attributed to the bag temperature which is generating the same amount of bag constant as

$$B_{\rm bag} = \frac{37}{30}\pi^2(T_{\rm bag})^4, \tag{23}$$

and the related temperature is about 14 MeV. Using this assumption, the energy density from Eq. (21) becomes

$$\varepsilon = \frac{37}{30}\pi^2\left(T^4 + T_B^4\right), \tag{24}$$

and the temperature will be equal to

$$T = \left(\frac{30}{37\pi^2}(\varepsilon - B_{\rm bag})\right)^{1/4}. \tag{25}$$

The background temperature T_0 is related to the background energy density of the medium ε_0 through (25), i.e., $T_0 = [30/37\pi^2(\varepsilon_0 - B_{\rm bag})]^{1/4}$. By replacing (25) into Eq. (22) the entropy density is obtained as a function of energy density as follows:

$$s = s(\varepsilon) = 4\frac{37}{90}\pi^2\left(\frac{30}{37\pi^2}(\varepsilon - B_{\rm bag})\right)^{3/4}. \tag{26}$$

We take the beam direction along the z axis. Therefore the transverse momentum of produced particles after the interaction will be on the $x-y$ plane. If we neglect the deflections due to elliptic flow, in the center of the mass coordinates, the system can be expressed by the longitudinal proper time and transverse momentum. The momentum distribution function on the transverse plane is a symmetric function of radial distance, i.e., $v = v(r)$.

Substituting (21) and (26) into (11) the one-dimensional relativistic continuity equation for entropy density is achieved

$$(1-v^2)\left[\left(\frac{90}{148\pi^2T^4}\right)\left(\frac{\partial\varepsilon}{\partial t} + v\frac{\partial\varepsilon}{\partial r}\right) + \frac{\partial v}{\partial r} + \frac{v}{r}\right] + v\left(\frac{\partial v}{\partial t} + v\frac{\partial v}{\partial r}\right) = 0. \tag{27}$$

The relation between energy density and pressure from Eq. (21) is found as

$$\varepsilon + p = \frac{148}{90}\pi^2T^4. \tag{28}$$

According to Eq. (28) and remembering that $\frac{\partial p}{\partial t} = \frac{1}{3}\frac{\partial\varepsilon}{\partial t}$ and using $\vec{\nabla}p = \frac{1}{3}\vec{\nabla}\varepsilon$, the relativistic Euler equation in (1+1) dimensions is obtained as

$$\frac{148}{30}\pi^2T^4\left(\frac{\partial v}{\partial t} + v\frac{\partial v}{\partial r}\right) - (v^2-1)\left(\frac{\partial\varepsilon}{\partial r} + v\frac{\partial\varepsilon}{\partial t}\right) = 0. \tag{29}$$

Now we have a complete set of equations for studying the time evolution of the propagating waves in the QGP.

IV. HEAD-ON COLLISION IN A QUARK GLUON PLASMA WITH CYLINDRICAL SYMMETRY

Hydrodynamics equations with cylindrical symmetry on the transverse plane and longitudinal scaling flows are usually applied to calculate the dynamics of the propagated waves in the central heavy ion collisions. So we expand our derived equations in cylindrical coordinates. Let us rewrite Eqs. (27) and (29) by dimensionless variables,

$$\hat{\varepsilon} = \frac{\varepsilon}{\varepsilon_0}, \quad \hat{v} = \frac{v}{c_s}, \tag{30}$$

where ε_0 is the equilibrium energy density of the QGP. Evolution equations of the system are nonlinear, and so we cannot find an exact solution, so we have to solve them numerically. We try to find a simplified equation for the propagation of small amplitude waves in the QGP. We can investigate the medium properties from characters of such traveling waves. The "stretched coordinates" approach is a powerful technique for this purpose. We have used the small dimensionless parameter σ to expand the variables and parameters of the system as a power series of σ [36–38]. Hence Eq. (30) can be written in terms of σ as [36]

$$\hat{\varepsilon} = 1 + \sigma^2\varepsilon_1 + \sigma^3\varepsilon_2 + \cdots,$$
$$\hat{v} = \sigma^2 v_1 + \sigma^3 v_2 + \cdots. \tag{31}$$

The stretched coordinates for describing the head-on collision of the traveling waves are introduced as follows:

$$\xi = \sigma(r - c_1 t) + \sigma^2 P_0(\eta,\tau) + \sigma^3 P_1(\eta,\xi,\tau),$$
$$\eta = \sigma(r + c_2 t) + \sigma^2 Q_0(\xi,\tau) + \sigma^3 Q_1(\xi,\eta,\tau),$$
$$\tau = \sigma^3 t. \tag{32}$$

Now by substituting Eqs. (30)–(32) into (27) and (29), the first nonzero term with respect to σ leads to

$$\frac{90\varepsilon_0}{148\pi^2T^4}\left(-c_1\frac{\partial\varepsilon_1}{\partial\xi} + c_2\frac{\partial\varepsilon_1}{\partial\eta}\right) + c_s\frac{\partial v_1}{\partial\xi} + c_s\frac{\partial v_1}{\partial\eta} = 0, \tag{33}$$

and

$$\frac{148\pi^2T^4c_s}{30}\left(-c_1\frac{\partial v_1}{\partial\xi} + c_2\frac{\partial v_1}{\partial\eta}\right) + \varepsilon_0\frac{\partial\varepsilon_1}{\partial\xi} + \varepsilon_0\frac{\partial\varepsilon_1}{\partial\eta} = 0. \tag{34}$$

Variables ε_1 and v_1 can be grouped into two different terms, one depending on ξ and τ and the other, a function of η and τ as $\varepsilon_1 = \varepsilon_1^1(\xi,\tau) + \varepsilon_1^2(\eta,\tau)$ and $v_1 = v_1^1(\xi,\tau) + v_1^2(\eta,\tau)$. If we apply these assumptions into Eqs. (33) and (34) we find

$$\frac{90\varepsilon_0}{148\pi^2T^4}\left(-c_1\frac{\partial\varepsilon_1^1}{\partial\xi} + c_2\frac{\partial\varepsilon_1^2}{\partial\eta}\right) + c_s\frac{\partial v_1^1}{\partial\xi} + c_s\frac{\partial v_1^2}{\partial\eta} = 0, \tag{35}$$

and

$$\frac{148\pi^2T^4c_s}{30}\left(-c_1\frac{\partial v_1^1}{\partial\xi} + c_2\frac{\partial v_1^2}{\partial\eta}\right) + \varepsilon_0\frac{\partial\varepsilon_1^1}{\partial\xi} + \varepsilon_0\frac{\partial\varepsilon_1^2}{\partial\eta} = 0. \tag{36}$$

The velocity can be found in terms of energy density as

$$v_1 = \frac{90\varepsilon_0}{148\pi^2T^4c_s}\left(c_1\varepsilon_1^1 - c_2\varepsilon_1^2\right). \tag{37}$$

Also the phase velocities are earned as

$$c_1^2 = c_2^2 = \tfrac{1}{3}. \tag{38}$$

The second order of expansions in Eqs. (33) and (34) leads to the same result when the index "1" is replaced by "2" and vice versa. By inserting (37) and (38) into (33) and (34) and collecting the terms of order σ^3 we have

$$\frac{90\varepsilon_0}{148\pi^2T^4}\left\{\begin{array}{l}\left(\frac{\partial\varepsilon_1^1}{\partial\tau} + \frac{\partial\varepsilon_1^2}{\partial\tau} - 2c_2Q_{0\xi}\frac{\partial\varepsilon_1^2}{\partial\eta} + 2c_1P_{0\eta}\frac{\partial\varepsilon_1^1}{\partial\xi} - c_1\frac{\partial\varepsilon_3}{\partial\xi} + c_2\frac{\partial\varepsilon_3}{\partial\eta} + \frac{\varepsilon_1^1}{\tau} - \frac{\varepsilon_1^2}{\tau}\right)\\ + \frac{30\varepsilon_0}{74\pi^2T^4}\left(c_1\varepsilon_1^1\frac{\partial\varepsilon_1^1}{\partial\xi} - c_2\varepsilon_1^2\frac{\partial\varepsilon_1^1}{\partial\xi} + c_1\varepsilon_1^1\frac{\partial\varepsilon_1^2}{\partial\eta} - c_2\varepsilon_1^2\frac{\partial\varepsilon_1^2}{\partial\eta}\right)\end{array}\right\} + c_s\frac{\partial v_3}{\partial\xi} + c_s\frac{\partial v_3}{\partial\eta} = 0, \tag{39}$$

and

$$3\varepsilon_0\left(c_1\frac{\partial\varepsilon_1^1}{\partial\tau}-c_2\frac{\partial\varepsilon_1^2}{\partial\tau}\right)+2\varepsilon_0 Q_{0\xi}\frac{\partial\varepsilon_1^2}{\partial\eta}+2\varepsilon_0 P_{0\eta}\frac{\partial\varepsilon_1^1}{\partial\xi}+\varepsilon_0\frac{\partial\varepsilon_3}{\partial\xi}+\varepsilon_0\frac{\partial\varepsilon_3}{\partial\eta}+\frac{30\varepsilon_0^2}{74\pi^2T^4}\left(\varepsilon_1^1\frac{\partial\varepsilon_1^1}{\partial\xi}-\varepsilon_1^2\frac{\partial\varepsilon_1^1}{\partial\xi}-\varepsilon_1^1\frac{\partial\varepsilon_1^2}{\partial\eta}+\varepsilon_1^2\frac{\partial\varepsilon_1^2}{\partial\eta}\right)-\frac{148\pi^2T^4c_s}{30}\left(c_1\frac{\partial v_3}{\partial\xi}-c_2\frac{\partial v_3}{\partial\eta}\right)=0. \tag{40}$$

Differentiating Eqs. (39) and (40) with respect to ξ and η, we will find four different equations. Combining these new equations and using (38) we obtain

$$\frac{\partial}{\partial\xi}\left(6c_1\frac{\partial\varepsilon_1^1}{\partial\tau}+2\frac{60\varepsilon_0}{148\pi^2T^4}\varepsilon_1^1\frac{\partial\varepsilon_1^1}{\partial\xi}+3c_1\frac{\varepsilon_1^1}{\tau}\right)-\frac{\partial}{\partial\eta}\left(6c_2\frac{\partial\varepsilon_1^2}{\partial\tau}-2\frac{60\varepsilon_0}{148\pi^2T^4}\varepsilon_1^2\frac{\partial\varepsilon_1^2}{\partial\eta}-3c_2\frac{\varepsilon_1^2}{\tau}\right)+\frac{\partial}{\partial\eta}\left[\left(4Q_{0\xi}-2\frac{60\varepsilon_0}{148\pi^2T^4}\varepsilon_1^1\right)\frac{\partial\varepsilon_1^2}{\partial\eta}\right]+\frac{\partial}{\partial\xi}\left[\left(4P_{0\eta}-2\frac{60\varepsilon_0}{148\pi^2T^4}\varepsilon_1^2\right)\frac{\partial\varepsilon_1^1}{\partial\xi}\right]+4\frac{\partial^2\varepsilon_3}{\partial\xi\,\partial\eta}=0. \tag{41}$$

Finally by considering the dependency of ε_1^1 and ε_1^2 on the variables τ, ξ, and η, we find

$$\frac{\partial\varepsilon_1^1}{\partial\tau}+\frac{15\varepsilon_0}{37\pi^2T^4}c_1\varepsilon_1^1\frac{\partial\varepsilon_1^1}{\partial\xi}+\frac{\varepsilon_1^1}{2\tau}=0, \tag{42}$$

$$\frac{\partial\varepsilon_1^2}{\partial\tau}-\frac{15\varepsilon_0}{37\pi^2T^4}c_2\varepsilon_1^2\frac{\partial\varepsilon_1^2}{\partial\eta}-\frac{\varepsilon_1^2}{2\tau}=0, \tag{43}$$

$$Q_{0\xi}=\frac{15\varepsilon_0}{74\pi^2T^4}\varepsilon_1^1, \tag{44}$$

$$P_{0\eta}=\frac{15\varepsilon_0}{74\pi^2T^4}\varepsilon_1^2. \tag{45}$$

Equations (42) and (43) are wave equations which are functions of (ξ,τ) and (η,τ) describing the space-time evolution of energy density lumps in cylindrical coordinates. These equations are not symmetric as the signs of the last terms are opposite. For a specific point, such as the locations in which $\frac{\partial\hat{\varepsilon}_1^1}{\partial r}=\frac{\partial\hat{\varepsilon}_1^2}{\partial r}=0$, $\frac{\partial\varepsilon_1^1}{\partial\tau}<0$, whereas $\frac{\partial\varepsilon_1^2}{\partial\tau}>0$. This means that $\varepsilon_1^1(\varepsilon_1^2)$ decreases (increases) in time. $P_{0\eta}$ and $Q_{0\xi}$ are phase shifts of the localized waves after their head-on collision. The derived wave equations in $r-t$ space are derived from (32) as follows:

$$\frac{\partial\hat{\varepsilon}_1^1}{\partial t}+c_1\frac{\partial\hat{\varepsilon}_1^1}{\partial r}+\frac{15\varepsilon_0}{37\pi^2T^4}c_1\hat{\varepsilon}_1^1\frac{\partial\hat{\varepsilon}_1^1}{\partial r}+\frac{\hat{\varepsilon}_1^1}{2t}+\frac{15\varepsilon_0}{74\pi^2T^4}\hat{\varepsilon}_1^2\times\left(\frac{\partial\hat{\varepsilon}_1^1}{\partial t}-c_2\frac{\partial\hat{\varepsilon}_1^1}{\partial r}+\frac{\hat{\varepsilon}_1^1}{2t}\right)=0, \tag{46}$$

and

$$\frac{\partial\hat{\varepsilon}_1^2}{\partial t}-c_2\frac{\partial\hat{\varepsilon}_1^2}{\partial r}-\frac{15\varepsilon_0}{37\pi^2T^4}c_2\hat{\varepsilon}_1^2\frac{\partial\hat{\varepsilon}_1^2}{\partial r}-\frac{\hat{\varepsilon}_1^2}{2t}+\frac{15\varepsilon_0}{74\pi^2T^4}\hat{\varepsilon}_1^1\left(\frac{\partial\hat{\varepsilon}_1^2}{\partial t}+c_1\frac{\partial\hat{\varepsilon}_1^2}{\partial r}-\frac{\hat{\varepsilon}_1^2}{2t}\right)=0, \tag{47}$$

where $\hat{\varepsilon}_1^1=\sigma^2\varepsilon_1^1$ and $\hat{\varepsilon}_1^2=\sigma^2\varepsilon_1^2$ are small perturbations in the energy density. These equations clearly show that two localized waves (with amplitudes on the order of σ) travel toward each other and undergo a head-on collision.

V. NUMERICAL METHOD

The breaking wave Eqs. (46) and (47) in flat geometry can be rewritten in the general form of

$$\frac{\partial\hat{\varepsilon}}{\partial t}+c\frac{\partial\hat{\varepsilon}}{\partial x}+\alpha\hat{\varepsilon}\frac{\partial\hat{\varepsilon}}{\partial x}=0, \tag{48}$$

where c and α are the pulse velocity and a nonlinear coefficient, respectively. This equation describes the one-dimensional evolution of the first-order perturbation in the energy density of hot QGPs. The nonlinear coefficient α is a function of equilibrium energy density and the temperature as $\alpha=\pm\frac{15\varepsilon_0}{37\pi^2T^4}c=\pm\frac{c}{2}[1+(\frac{T_{\rm bag}}{T})^4]$ where the positive (negative) sign corresponds to the propagating waves in the direction (opposite direction) of the coordinate axis.

Since the last equations are nonlinear and there is no analytical solution for them, in this article Eqs. (46) and (47) are solved numerically. The finite difference approach is used to solve the partial differential system of equations (PDE). Due to the time term in the equations the problem is transient. Although there is no known exact solution for (46) and (47), we can examine the localized solutions of the KdV equation as an initial condition for the numerical solution as $\varepsilon(r,t=0)=A\ \mathrm{sec}\ h^2(r/\Delta)$ for energy density in nonplanar geometry, where A is the initial amplitude and Δ is its width [21]. In this case, since a direct computation of the time variable can be performed in terms of spatial (r) and some known quantities, it is possible to perform the numerical calculations explicitly as follows:

$$\hat{\varepsilon}^{n+1}=\hat{\varepsilon}^n+dtf\left(\frac{\partial\hat{\varepsilon}}{\partial r},r,\alpha\right). \tag{49}$$

We want to compute $\hat{\varepsilon}$ at the $(n+1)$th time-step (dt) in terms of its known value at the old time-step ($t=n\,dt$) with some changes. The idea of the finite difference method is to substitute the derivatives appearing in the PDE by finite differences, i.e., discrete terms that approximate them. In this paper for time and spatial discretizations, we use a central differencing scheme. By applying the central differencing scheme we can benefit the second-order accuracy. In our case (inviscid flow equations), the central differencing scheme is conditionally stable and depends on numerical parameters, such as pulse velocity (c), time step (dt), and grid size (dx). It is possible to define a nondimensional parameter for controlling the stability $\lambda=\frac{cdt}{dx}$. Our results show that one should use $\lambda\leqslant\frac{1}{2}$ in order to ensure stability and accuracy. Additionally the central differencing schemes applied to the inviscid equations

inherently introduce numerical dispersion near sharp changes as a deformed profile. Sometimes these undesirable numerical dispersions may interfere with the physical behavior, thereby humiliating the fidelity of the results [30]. Of course the central differencing scheme is not affected by artificial dissipation and so is favored as an accurate and efficient numerical method. For controlling these undesirable numerical dispersions we benefit from a kind of filter using the weighted average as below,

$$f(i)_{\text{filtered}} = \frac{f(i-1) + 2f(i) + f(i+1)}{4}. \qquad (50)$$

VI. DISCUSSION

Cold QGP matter is expected to exist in the core of ultradense neutron and quark stars because of squeezing due to high pressure. In such situations the temperature is low, i.e., $T_0 = T_{\text{bag}}$, and the nonlinear coefficient becomes $\alpha = \pm c$. Other important terms in Eqs. (46) and (47) are $\frac{\hat{\varepsilon}_1^1}{2t}$ and $\frac{\hat{\varepsilon}_1^2}{2t}$ which come from cylindrical geometry. If we write the continuity and the Navier-Stokes equations in nonplanar coordinates, an extra term (in comparison with the Cartesian coordinate) will appear as $\frac{n\hat{\varepsilon}}{2t}$ with $n = 1\,(n = 2)$ for cylindrical (spherical) symmetry. It is clear that for the Cartesian coordinate, $n = 0$, and this term is absent. This term is called the geometric term in literature [39,40]. Adding this term to (48) gives the full evolution equation in nonplanar geometry with cylindrical symmetry which is created in the central rapidity region of a typical heavy ion collision. At the beginning of the perturbation evolution, the effects of the geometric terms are considerable. It may be noted that these terms are singular at $t = 0$ [39–41]. For $|t| \gg 1$ these terms are sufficiently small, so Eqs. (46) and (47) reduce to (48) for sufficiently large values of time, whereas these terms become very large at $|t| \to 0$.

The KdV equation has an extra dispersive term in comparison with the breaking wave Eq. (48). This term compensates the effects of the nonlinear term and therefore stabilizes the KdV solutions as solitary waves. Therefore in general we can conclude that the propagating waves in the QGP media are not stable. But such perturbations can affect the boundary of the medium if they are able to reach there. So we have to study the shape of the moving lumps and their traveling distances before decay.

Equations (44) and (45) present the phase shifts of moving waves after their head-on collision. These equations indicate that waves with larger amplitude have smaller absolute values of phase shift.

Two concepts are introduced for a better explanation of the figures and the physics behind the figures. One of these two concepts is the "deformed" profile. In the current paper, the drastic change in the wave profile in a very small space interval (dr), i.e., a large gradient $(\frac{\partial \varepsilon}{\partial r})$, is introduced and used as the deformed profile. The other concept is the solitary wave life. As is known in mathematics and physics, a solitary wave is a kind of symmetrical wave which maintains its shape while it propagates at a constant velocity. When the symmetrical form of the solitary wave changes into the deformed wave, it is assumed that the lifetime of the solitary wave ends.

Figure 2 shows the time evolution of the propagating wave at a low-temperature medium as $T_0 = T_{\text{bag}}$ in cylindrical geometry. The initial position of the solitary waves has been taken as $r_{01} = 3.0$ and $r_{02} = 5.0$ fm, and their initial width is $\Delta = 0.1$. Amplitudes of the left (right) profile in Fig. 2(a) are taken $A = 0.0625$ $(A = 0.035)$ and in Fig. 2(b) have been taken as $A = 0.1$ $(A = 0.0625)$. As previously stated, due to the singularity of $\frac{\hat{\varepsilon}_1^1}{2t}$ and $\frac{\hat{\varepsilon}_1^2}{2t}$ at $t = 0$, the calculations for the time evolution of the moving waves should be performed at longer times, therefore we have started our simulations from $t = 0.5\,\text{fm}/c$ after the heavy ion collision. These figures clearly show that the amplitude of the upward moving solitary wave reduces in time whereas the amplitude of the downward moving wave increases rapidly. These figures indicate that the shapes of the localized perturbations spoil in time. Comparison of Figs. 2(a) and 2(b) shows that the solitary wave lifetime

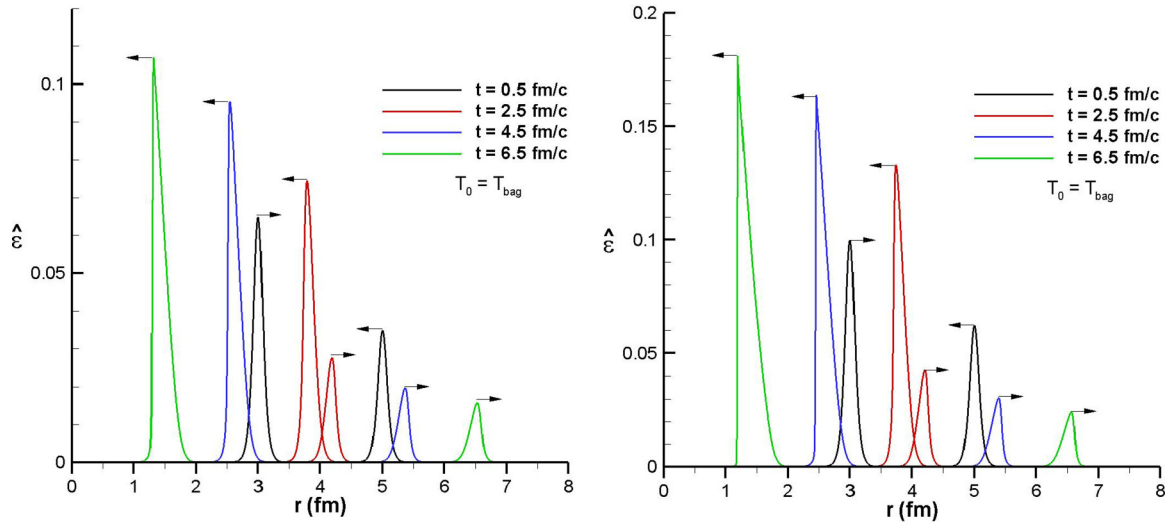

FIG. 2. Time evolution of two energy density pulses at $T_0 = T_{\text{bag}}$ with cylindrical symmetry. Initial amplitudes of the solitons of (a) the left panel are 0.0625, 0.035, and $\Delta = 0.1$ whereas in (b) the right panel they are 0.1, 0.0625, and $\Delta = 0.1$.

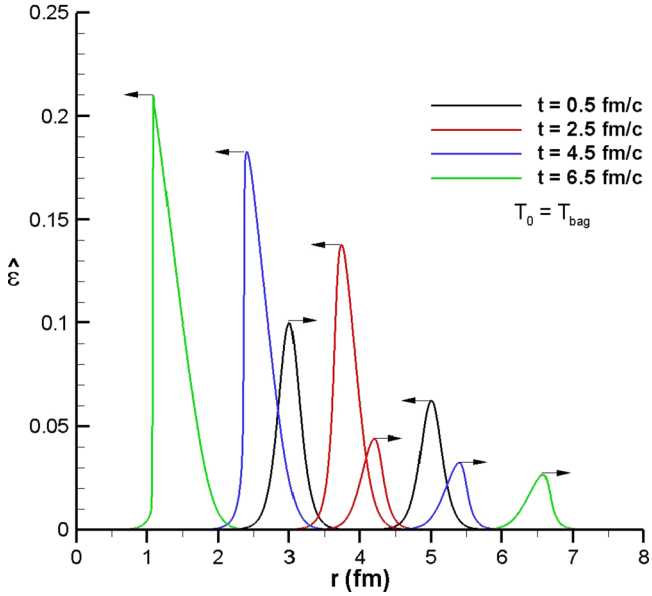

FIG. 3. Time evolution of two energy density pulses at $T = T_{\text{bag}}$ with cylindrical symmetry. Initial amplitude and width of the left (right) soliton are $A = 0.1$ and $\Delta = 0.2$ ($A = 0.0625$ and $\Delta = 0.2$).

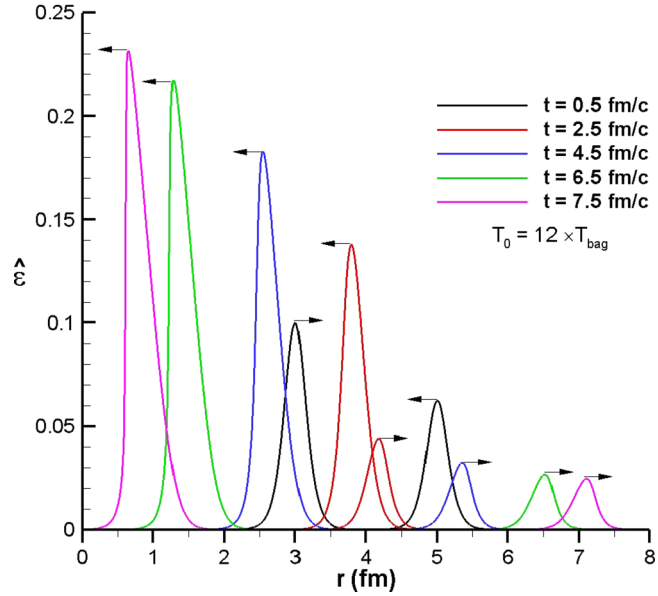

FIG. 4. Evolution of colliding solitary waves for $T_0 = 12T_{\text{bag}}$ in the range of RHIC temperature.

decreases when the amplitude of the initial waves increases. T_0 is the background temperature which is a function of the energy density described by (24). It may be noted that such a scale of temperature is related to the cold hadronic matter. They live long enough to travel distances on the order of 10 fm. Such distances are not of interest in the physics of dense astronomical objects. On the other hand, heavy ion collisions are very hot and $T_0 \gg T_{\text{bag}}$, but the dimension of the fireballs in RHIC and LHC are assumed to be about 6–10 fm [42].

Figure 3 presents a head-on collision of moving solitons with the same amplitudes of Fig. 2(b) but different in width. This figure indicates that wider solitons are more stable during the downward movement. Indeed solitary profiles with greater slopes (larger amplitude and smaller width) will spoil sooner.

The maximum value of the nonlinear coefficient is $\alpha = c$ which occurs in cold hadronic matter. In high relativistic heavy ion collisions medium temperature (background energy density) is much higher than the bag temperature (bag energy). Therefore the nonlinear coefficient α becomes smaller, and therefore it is expected that localized waves pass longer distances in the medium. Our simulations show that in the case of $T \gg T_{\text{bag}}$ ($\varepsilon \gg \varepsilon_{\text{bag}}$) solitary waves are able to travel distances much longer than the size of the fireball after their head-on collision.

Figure 4 demonstrates the time evolution of colliding waves with similar identifications of Fig. 3 but for $T_0 = 12T_{\text{bag}}$ in the range of the temperature of the heavy ion collisions. This figure shows that, for higher temperatures, solitary waves are more stable, and they are able to pass the fireball and create detectable effects at the borders. As stated before, the amplitude of the right moving solitary waves becomes smaller whereas the left moving one becomes larger. Therefore we will have two colliding waves with different amplitudes at the borders which emit energy in the same line but opposite directions. Figure 4 demonstrates that traveling waves will not become spoiled within short periods as compared with solitary waves in cold hadronic matter.

According to the above procedure we have performed several numerical calculations with different initial conditions. We have evaluated the solution during time periods in which the numerical errors are small. Figures 2–4 clearly show that the solitary profiles smoothly change during the evolution. Our findings clearly indicate that the periodical breaking profiles as reported in some papers [30,37,38,43] are due to numerical instabilities. Indeed there is no physical reason for creating periodical breaking profiles.

VII. CONCLUSIONS AND REMARKS

In this paper we have investigated the propagation of small amplitude localized waves in a dense quark gluon plasma which is produced in the center of relativistic heavy ion collisions or exists in the core of superdense astronomical objects. The MIT bag model has been used to describe the equation of state of the quark gluon plasma. A hydrodynamics equation and a suitable equation of state have been linearized using the reductive perturbation method. We showed that perturbations in energy density are propagated in the medium as localized waves which move toward each other. Using numerical calculations we find that localized perturbations in hot quark gluon plasma travel longer distances in comparison with cold hadronic matter before changing into deformed profiles. Hence localized waves travel longer distances in higher-temperature QGPs and live long enough to reach the borders of the medium. So they can create detectable effects at the detectors. Also we have derived the higher-order analytical phase shifts after the collisions which are proportional to the

amplitudes of two collisional waves. It is shown that incident waves reach the borders with different amplitudes.

In this paper we have considered a Fermi-Dirac distribution function for the matter under investigation. Some studies indicate that the nonextensive distribution function is a better model for describing the distribution of plasma constituents in different equations of state of the QGP. Such a situation can be considered in future works.

In the heavy ion collisions with energy in the range of 100-A MeV–10-A GeV nuclei projectiles absorb each other, and the nuclear matter is compressed, heated, and produces a QGP in a spatial region with spherical-like symmetry. The results in this range of energy have astrophysical relevance to compact neutron star explosions [44]. One can investigate such a situation by solving the presented model in spherical geometry.

[1] L. Del Zanna, V. Chandra, G. Inghirami, V. Rolando, A. Beraudo, A. De Pace, G. Pagliara, A. Drago, and F. Becattini, Eur. Phys. J. **73**, 2524 (2013).

[2] H. J. Drescher, F. M. Liu, S. Ostapchenko, T. Pierog, and K. Werner, Phys. Rev. C **65**, 054902 (2002).

[3] G. Sarwar and J. E. Alam, arXiv:1503.06019v2 [nucl-th].

[4] J. P. Blaizotand and J. Y. Ollitrault, Phys. Lett. B **191**, 21 (1987).

[5] L. McLerran, Rev. Mod. Phys **58**, 1021 (1986).

[6] D. Enstrom, arXiv:hep-ph/9802337.

[7] N. K. Glendenning and T. Matsui, Phys. Lett. B **141**, 419 (1984).

[8] K. Yagi, T. Hatsuda, and Y. Miake, *Quark-Gluon Plasma: From Big Bang to Little Bang* (Cambridge University Press, Cambridge, UK, 2005).

[9] H. Satz, Nucl. Phys. **A862-863**, 4 (2011).

[10] J. D. Rameau, T. J. Reber, H.-B. Yang, S. Akhanjee, G. D. Gu, P. D. Johnson, and S. Campbell, Phys. Rev. B **90**, 134509 (2014).

[11] L. A. Linden Levy, J. L. Nagle, C. Rosen, and P. Steinberg, Phys. Rev. C **78**, 044905 (2008).

[12] G. Torrieri, B. Tomášik, and I. Mishustin, Phys. Rev. C **77**, 034903 (2008).

[13] H. Kouno, M. Maruyama, F. Takagi, and K. Saito, Phys. Rev. D **41**, 2903 (1990).

[14] J. P. Blaizot and J. Y. Ollitrault, Phys. Rev. D **36**, 916 (1987).

[15] C. Manuel and S. Mrówczyński, Phys. Rev. D **68**, 094010 (2003).

[16] P. Staig and E. Shuryak, Phys. Rev. C **84**, 044912 (2011).

[17] P. Staig and E. Shuryak, Phys. Rev. C **84**, 034908 (2011).

[18] St. Mrówczyński, E. V. Shuryak, and E. V. Shuryak, Acta Phys. Pol. **34**, 4241 (2003).

[19] S. Mrówczyński, Phys. Rev. C **57**, 1518 (1998).

[20] J. I. Kapusta, B. Müller, and M. Stephanov, Phys. Rev. C **85**, 054906 (2012).

[21] D. A. Fogaça, F. S. Navarra, and L. G. Ferreira Filho, Phys. Rev. C **88**, 025208 (2013).

[22] E. Shuryak and P. Staig, Phys. Rev. C **88**, 064905 (2013).

[23] P. Chakraborty, M. G. Mustafa, and M. H. Thoma, Phys. Rev. D **68**, 085012 (2003).

[24] M. Stephanov, K. Rajagopal, and E. Shuryak, Phys. Rev. Lett. **81**, 4816 (1998).

[25] M. Stephanov, K. Rajagopal, and E. Shuryak, Phys. Rev. D **60**, 114028 (1999).

[26] A. Y. Abul-Magd, I. El-Taher, and F. M. Khaliel, Phys. Rev. C **45**, 448 (1992).

[27] D. A. Fogaça and F. S. Navarra, Nucl. Phys. A **790**, 619c (2007).

[28] F. S. Navarra, D. A. Fogaça, and L. G. Ferreira Filho, Nucl. Phys. B, Proc. Suppl. **199**, 337 (2010).

[29] A.-M. Wazwaz, *Partial Differential Equations and Solitary Waves Theory* (Springer, Dordrecht, 2010).

[30] D. A. Fogaça, L. G. Ferreira Filho, and F. S. Navarra, Phys. Rev. C **81**, 055211 (2010).

[31] A. Rafiei and K. Javidan, Astrophys. Space Sci. **357**, 10 (2015).

[32] J. Y. Ollitrault, Eur. J. Phys. **29**, 275 (2008).

[33] N. Arbex, U. Ornik, M. Plümer, and R. M. Weiner, Phys. Rev. C **55**, 860 (1997).

[34] A. Chodos, R. L. Jaffe, K. Johnson, C. B. Thorn, and V. F. Weisskopf, Phys. Rev. D **9**, 3471 (1974).

[35] J. Gu, H. Guo, X. Li, Y. Liu, and F. Xu, Phys. Rev. C **73**, 055803 (2006).

[36] E. Infeld and G. Rowlands, *Nonlinear Waves, Solitons and Chaos* (Cambridge University Press, Cambridge, UK, 2000).

[37] D. A. Fogaça, F. S. Navarra, and L. G. Ferreira Filho, Phys. Rev. D **84**, 054011 (2011).

[38] D. A. Fogaça, F. S. Navarra, and L. G. Ferreira Filho, Commun. Nonlinear. Sci. Numer. Simul. **18**, 221 (2013).

[39] S. Tasnim, S. Islam, and A. A. Mamun, Phys. Plasmas **19**, 033706 (2012).

[40] H. R. Pakzad, K. Javidan, and M. Tribeche, Astrophys. Space Sci. **352**, 185 (2014).

[41] K. Javidan, Astrophys. Space Sci. **343**, 667 (2013).

[42] ALICE Collaboration, Phys. Lett. B **696**, 328 (2011).

[43] D. A. Fogaça, L. G. Ferreira Filho, and F. S. Navarra, Nucl. Phys. A **819**, 150 (2009).

[44] L. P. Csernai and D. D. Strottman, in *International Review of Nuclear Physics: Relativistic Heavy Ion Physics*, edited by T. Engeland, J. Rekstad, and J. S. Vaagen (World Scientific, Singapore, 1991), Vol. 2.